4122–4135 *Nucleic Acids Research, 2011, Vol. 39, No. 10* *Published online 29 January 2011*
doi:10.1093/nar/gkr005

Biophysical analysis and small-angle X-ray scattering-derived structures of MeCP2–nucleosome complexes

Chenghua Yang[1], Mark J. van der Woerd[1], Uma M. Muthurajan[1], Jeffrey C. Hansen[1] and Karolin Luger[2,*]

[1]Department of Biochemistry and Molecular Biology and [2]Howard Hughes Medical Institute, Colorado State University, Fort Collins, CO 80523-1870, USA

Received June 7, 2010; Revised and Accepted January 1, 2011

ABSTRACT

MeCP2 is a highly abundant chromatin architectural protein with key roles in post-natal brain development in humans. Mutations in MeCP2 are associated with Rett syndrome, the main cause of mental retardation in girls. Structural information on the intrinsically disordered MeCP2 protein is restricted to the methyl-CpG binding domain; however, at least four regions capable of DNA and chromatin binding are distributed over its entire length. Here we use small angle X-ray scattering (SAXS) and other solution-state approaches to investigate the interaction of MeCP2 and a truncated, disease-causing version of MeCP2 with nucleosomes. We demonstrate that MeCP2 forms defined complexes with nucleosomes, in which all four histones are present. MeCP2 retains an extended conformation when binding nucleosomes without extra-nucleosomal DNA. In contrast, nucleosomes with extra-nucleosomal DNA engage additional DNA binding sites in MeCP2, resulting in a rather compact higher-order complex. We present *ab initio* envelope reconstructions of nucleosomes and their complexes with MeCP2 from SAXS data. SAXS studies also revealed unexpected sequence-dependent conformational variability in the nucleosomes themselves.

INTRODUCTION

Methyl-CpG binding protein 2 (MeCP2) is a chromatin-associated protein that is highly abundant in neuronal cells, amounting to about one MeCP2 molecule for every two nucleosomes (1). Mutations in the coding region of MeCP2 lead to Rett syndrome (RTT), a neuro-developmental disease which is the main cause of mental retardation and autistic behaviour in girls [reviewed in ref. (2)]. The incidence of RTT is about 1 in every 10 000–15 000 female births (3). MeCP2 is also implicated in multiple other developmental disorders, suggesting that it occupies a central role in the post-natal development of the human brain (4). There are currently over 200 mutations found in the MeCP2 gene that cause RTT, most of which cluster around eight 'hot spots' distributed throughout the protein sequence (Figure 1). Four of the five most frequent RTT-causing mutations introduce stop codons into the transcription repression domain (TRD); the fifth most frequent mutation terminates at the end of the TRD (R294X; http://mecp2.chw.edu.au/mecp2/). A recent view suggests that MeCP2 dysfunction induces changes in the expression levels of thousands of genes, with a majority of genes being activated by MeCP2 (5). This suggests that MeCP2 under normal cellular conditions might not act as a gene specific transcriptional regulator as previously assumed (6,7), but instead might dampen transcriptional noise genome-wide in a DNA methylation-dependent manner (1).

Human MeCP2 isoform e2 is composed of 486 amino acids and is a monomer in solution (8). Circular dichroism (CD) data of full length MeCP2 indicate that it is 60% unstructured (9), consistent with theoretical predictions [FoldIndex (http://bip.weizmann.ac.il/fldbin/findex)] (10). Limited protease digestion of full length MeCP2 has identified six 'domains' (9) (Figure 1). Two of these have been particularly well characterized functionally: the methyl-CpG binding domain (MBD) that binds both unmethylated and methylated DNA, spanning amino acids 76–163 (11) and the TRD (amino acids 203–310) (12). Stop codons between amino acids 168 and 294 are among the most frequently found mutations in RTT patients (http://mecp2.chw.edu.au/mecp2/). No mis-sense

*To whom correspondence should be addressed. Tel: +1 970 491 6405; Fax: +1 970 491 5113; Email: karolin.luger@colostate.edu

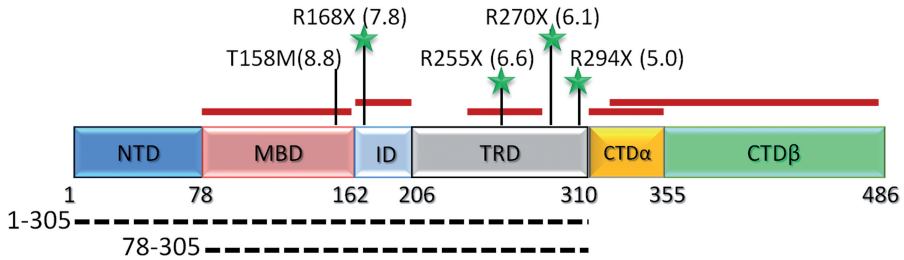

Figure 1. Domain structure of MeCP2. Dashed lines indicate the constructs used here, in addition to full length protein. NTD: N-terminal domain; MBD: methyl-CpG DNA binding domain, TRD: transcription repression domain, CTD: C-terminal domain. Red bars above indicate mapped DNA binding regions. The five most frequent mutations are indicated (percent occurrence given in brackets; nonsense mutations are indicated by asterisks).

mutations have been mapped to the NTD (amino acids 1–78). To date, structural information is only available for the MBD (amino acids 77–163) alone and in complex with a short fragment of methylated DNA (13,14). The other five MeCP2 domains are mostly unstructured as judged by both CD and theoretical predictions. Thus, MeCP2 falls into the category of proteins known as 'intrinsically disordered'. Traditional structural techniques such as X-ray crystallography and NMR cannot provide useful structural information for the full length protein.

The MBD of MeCP2 not only recognizes methylated DNA (15) but also binds unmethylated DNA (16,17). Additional unmethylated DNA binding sites (DBDs) have been mapped to the intervening domain (ID) between the MBD and TRD (17,18), the TRD (9,17) and the CTDα (Figure 1) (17). Thus, there are at least four regions spanning residues 77–354 that contribute to unmethylated DNA binding *in vitro*. MeCP2 also binds to nucleosomes and nucleosomal arrays *in vitro* (17,19) and to chromatin *in vivo* (18). Early *in vitro* studies claimed that MeCP2 forms discrete complexes with nucleosomes via the MBD in a methyl-CpG dependent manner. The carboxyl-terminal segment of MeCP2 contributes to binding both to free DNA and to the nucleosome and to MeCP2-dependent chromatin compaction (11,17). More recently it was demonstrated that MeCP2 interacts with higher affinity with nucleosomes with methylated DNA (17) and that the presence of the extra-nucleosomal 'linker' DNA in the nucleosome is essential for this interaction (20). MeCP2 protects an additional ~11 bp from digestion with micrococcal nuclease, indicating that the MeCP2 binding site on nucleosomes is close to the linker DNA entry–exit region. Electron microscopy of the MeCP2-nucleosome complexes may be interpreted as a nucleosome-MeCP2-nucleosome 'sandwich' structure in ~40% of the cases examined (20), consistent with multiple DNA binding sites on each MeCP2 monomer.

Binding of recombinant human MeCP2 to positioned nucleosomal arrays in the absence of DNA methylation promotes their compaction into highly condensed structures (16). However, how MeCP2-mediated chromatin compaction occurs is completely unknown. One recent view (supported by the high abundance of MeCP2 especially in neuronal cells) is that MeCP2 may function similar to linker histones (21) by serving as a key regulator of chromatin structure in neurons, thereby globally contributing to gene regulation. Thus, understanding how MeCP2 interacts with the nucleosome, the fundamental building block of eukaryotic chromatin, is essential to understand the function of this enigmatic protein in health and disease.

Here, we present a rigorous biophysical and biochemical analysis of the complexes formed between MeCP2 and nucleosomes without and with extra-nucleosomal linker DNA. We also analyse truncated versions of MeCP2 (encompassing amino acids 1–305 and 74–305, respectively) both of which serve as models for the fifth most frequent RTT mutant R294X. Our studies show that MeCP2 forms defined complexes with nucleosomes irrespective of the presence of extra-nucleosomal linker DNA. MeCP2 binds preferentially to nucleosomes with linker DNA by engaging additional DNA binding domains. We have obtained structural data of nucleosomes and MeCP2-nucleosome complexes from small-angle X-ray scattering (SAXS) experiments. From the SAXS experiments we identified different conformational states of nucleosomal DNA dependent on the DNA sequence used to form nucleosomes. Our SAXS data further allow us to hypothesize how MeCP2 might interact with nucleosomes and nucleosomal arrays to cause chromatin compaction.

Experimental procedures

Expression and purification of MeCP2. Recombinant full length human MeCP2 (isoform e2) was expressed in the IMPACT system (New England Biolabs) and purified as described (9). Purified full length MeCP2 and fragments 1–305 and 78–305 (Figure 1) were dialysed into storage buffer (10 mM Tris, pH 7.5, 10% glycerol, 10 mM NaCl, 0.25 mM EDTA, 1 mM β-mercaptoethanol) and stored at 4°C.

Nucleosomal DNA and nucleosome reconstitution. Either 147-bp palindromic DNA fragments derived from human α-satellite DNA (22) or 146- and 165-bp DNA fragments derived from the strong positioning '601' DNA sequence (23) were used (Supplementary Figure S1). Nucleosome reconstitution with recombinant histones was done as previously described (24), resulting in three types of nucleosomes referred to as A-Nuc147 (α-sat sequence); W-Nuc146 and W-Nuc165 (both '601' sequence), respectively.

Electrophoretic mobility shift assays. A-Nuc147 or W-Nuc165 (15 μM) were incubated with increasing

amounts of MeCP2 in 10 mM Tris, pH 7.5, 1 mM EDTA, 1 mM DTT and 0, 100 or 300 mM NaCl in 10 µl reaction volumes at room temperature for 30 min. The products were electrophoresed on pre-run 5% polyacrylamide gels (mono/bis ratio of 35:1) in 0.2X TB (45 mM Tris, 45 mM borate pH 8.3) at 150 V for 75 min at 4°C.

Nucleosome competition assay. W-Nuc146 was pre-incubated with MeCP2 at a 1–1.5 molar ratio in 10 mM Tris pH 7.5, 100 mM NaCl, 2% glycerol, 0.2 mM TCEP at room temperature for 30 min. Increasing amounts (0.25–1 molar ratio to W-Nuc146) of Alexa Fluor-488 labeled W-Nuc165 was added to the pre-incubated W-146Nuc-MeCP2 complex and incubated at room temperature for another 30 min before resolving on a 5% native PAGE gel. The reverse competition assay was done under identical conditions. The products were electrophoresed on pre-run 5% polyacrylamide gel as described above. The gel was visualized both by fluorescence and ethidium bromide staining. Competition assays with 53 bp DNA were performed under the same conditions.

Analytical ultracentrifugation. For sedimentation velocity experiments in the analytical ultracentrifuge, A-Nuc147 or W-Nuc165 alone or in complex with MeCP2 at the indicated molar ratios was prepared at ~600 nM. Sedimentation velocity experiments were performed at low salt concentration (10 mM Tris, pH 7.5, 1 mM EDTA, 1 mM DTT). Sedimentation velocity experiments were done in a Beckman XL-I or XL-A analytical ultracentrifuge with absorbance detection at 260 nm. Scans were collected at a radial step resolution of 0.003 cm at 25 000 rpm for 5 h. Boundaries were analysed using the Ultrascan software (version 7.3). This analysis gives a diffusion-corrected integral distribution of sedimentation coefficients, G(s). Sedimentation coefficients were corrected to that in water at 20°C. The solvent densities were calculated in Ultrascan (25). The partial specific volumes of the samples were calculated from the primary DNA and amino acid sequence within Ultrascan.

Size-exclusion chromatography/multi-angle light scattering. Size-exclusion chromatography combined with multi-angle light scattering (SEC-MALS) (Wyatt technologies) was performed at the Advanced Light Source (ALS) in Berkeley, California. A Superose-6 PC 3.2/30 column (2.4 ml total volume, GE Healthcare) with a flow rate of 40 µl/min was used to separate the sample before performing the MALS measurement. Experiments were done with 25 µl 11.5 µM of A-Nuc147 or W-Nuc165 alone or each of these in a 1:1 complex with MeCP2-WT in the same buffer as above (10 mM Tris, pH 7.5, 1 mM EDTA, 1 mM DTT). The same samples were used for SAXS (see below). They were at least 90% homogeneous as determined by electrophoretic mobility shift assays (EMSA). The molar mass for each molecule was determined with the ASTRA software (Wyatt Technologies). SEC-MALS is an accurate tool for determining the molar mass of proteins in solution. It is also an extremely sensitive method for detecting whether—and how much of—any aggregates have formed, because the light scattering response is directly proportional to the weight-averaged molar mass (MW) of the sample being measured, multiplied by the concentration (see application notes under http://www.wyatt.eu/index.php?id=proteins&L=0%27).

SAXS data collection and analysis. SAXS data for all samples were collected at the SIBYLS beam line (12.3.1) at the ALS (Berkeley) with an X-ray energy of 10 keV (λ = 1.2398 Å). A Mar CCD detector was used to record the scattering data. A 15 µl sample was placed in a 1 mm thick chamber with two windows of 25 µm mica. The distance between the sample and the detector was 1.5 m. Stock solutions of MeCP2, A-Nuc147, W-Nuc146 and W-Nuc165 each at 7.5 mg/ml, and MeCP2 in complex with W-Nuc146 or W-Nuc165 at 9.4 mg/ml (the concentration of nucleosome remains the same in the complex when compared with the control nucleosome sample) were prepared. Additional samples were prepared by diluting the stock solutions to two-third and one-third concentration with reference buffer (10 mM Tris, pH 7.5, 1 mM EDTA, 1 mM DTT). Additional experiments were performed on A-Nuc147 at higher dilution (final concentration 0.8 mg/ml).

The intensity curves (intensity as a function of momentum of transfer $s = 4\pi \sin(\theta)/\lambda$ with 2θ the total scattering angle) were measured at all concentrations, and corrected for buffer scattering. Repeat exposures were taken to check for radiation damage, while two different exposures, typically of 6 and 60 s in duration, were taken to optimize the signal-to-noise ratio and avoid detector saturation. Initial data processing was performed with the program PRIMUS (26). The radius of gyration, Rg, was estimated by Guinier analysis (27) in PRIMUS using low-angle data ($Rg < 1.3$); the maximum particle dimension was estimated by regularized indirect Fourier transform with the program AUTOGNOM, an automated version of GNOM (28), which provides the P(r) function. The P(r) function is a histogram of inter-atomic distances and goes to zero at the maximum intramolecular distance d_{max}. The P(r) functions were normalized by scaling the function to I_0 for each sample.

At least 10 low-resolution molecular envelopes were calculated from the scattering data for each model, using the program DAMMIN (29) in slow mode and superimposed using SUPCOMB, providing a normalized spatial discrepancy (NSD) value which is zero for identical objects and larger than one for objects that systematically differ from one another (30). Finally, the pre-aligned models were averaged with DAMAVER (31), giving an effective occupancy of each voxel. A convex shell of all models can be generated by keeping all occupied voxels, while filtering at half-maximal occupancy provides 'filtered' models. These models were used for all subsequent analyses. To visualize the results, the reconstructed models were converted to volumetric maps using real space convolution with a Gaussian kernel with the program Situs (32,33). A kernel width of 6 Å and voxel spacing of 1 Å were used. Molecular representations were made with VMD (34). An appropriate scale bar was added

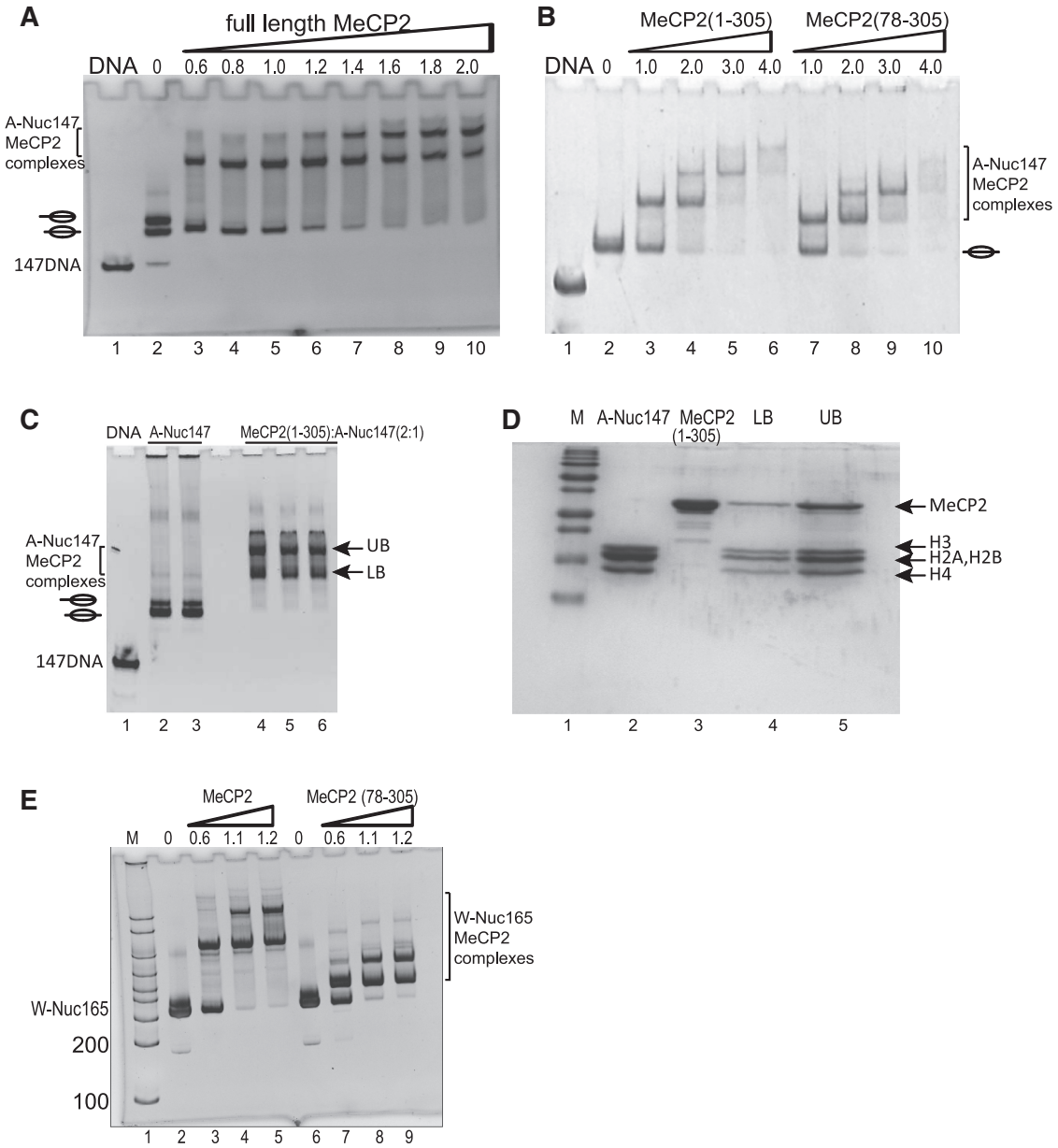

Figure 2. MeCP2 forms defined complexes with nucleosomes *in vitro*. Gels in (**A, B, C** and **E**) were stained in ethidium bromide, the gel in D was stained with Coomassie blue. (A) Increasing amounts of MeCP2 were added to A-Nuc147 resulting in retarded mobility of A-Nuc147. In this preparation, nucleosomes (in absence of MeCP2) migrate as two bands on the gel, representative of two different positions of the histone octamer with respect to the DNA (24). (B) Mobility shifts were also observed with MeCP2 N-terminal fragments (amino acids 1–305 or 78–305), indicating that the N-terminal portion of MeCP2 is sufficient for this interaction. (C and **D**) Upper and lower bands (C) were excised and eluted from the gel before loading onto an 18% SDS gel (D). (E) Electrophoretic mobility shifts were also observed with W-Nuc165, with both full length and the N-terminal MeCP2 (78–305) fragment.

to the final envelopes by displaying a ribbon scale in VMD and using this scale to generate the scale bars in final editing, so all images are shown on the same scale.

RESULTS

MeCP2 forms defined complexes with nucleosomes

Nucleosomes reconstituted with a 147 bp DNA fragment derived from α-sat DNA [A-Nuc-147; (22)] were incubated with increasing amounts of full length human recombinant MeCP2 and the complexes were resolved on a 5% native polyacrylamide gel (Figure 2A). The addition of increasing amounts of MeCP2 resulted in a progressive reduction of free A-Nuc147 and the appearance of discretely shifted and super-shifted bands. Nucleosomes in the off-centered position (Figure 2A, lane 2, upper band) shifted preferentially. The same behavior was observed with RTT MeCP2 fragments 1–305 or 78–305 (which encompasses the MBD, ID and TRD; Figure 2B), as well as with the individual MBD or TRD fragments (data not shown). Two bands

Table 1. SEC-MALS analysis of nucleosomes and nucleosome-MeCP2 complexes

Molecule or complex	SEC-MALS Molecular weight (kDa)	
	Observed (%)	Calculated
BSA	66.47 ± 2	67.0
MeCP2 full length	56.00 ± 4	52.44
A-Nuc147	198.0 ± 2	205.0
A-Nuc147-MeCP2 full length	251.4 ± 2	257.9 (1:1)
W-Nuc165	202.8 ± 1	208.95
W-Nuc165-MeCP2 full length	253.9 ± 0.6	261.4 (1:1)

Data were obtained from the experiments shown in Supplementary Figure S2. The observed and calculated values show a good correspondence and demonstrate that the complexes between nucleosomes and MeCP2 occur at a 1:1 ratio.

containing putative A-Nuc147-MeCP2$_{(1–305)}$ complexes were excised from the native gel (Figure 2C) and loaded onto an 18% SDS gel (Figure 2D). All four histones as well as MeCP2$_{(1–305)}$ were present in both bands. The relative intensities of the four core histones and MeCP2 bands are very similar in the two shifted complexes (Figure 2D, lanes 4 and 5). Because the upper shifted band reverts to the lower shifted band upon addition of more nucleosomes (data not shown), we interpret the upper super-shifted complex as having multiple MeCP2 molecules bound to one nucleosome. Similar MeCP2-nucleosome complexes were obtained after incubation in the presence of 150 and 300 mM NaCl (data not shown). Nucleosomes reconstituted with a 165 bp DNA fragment centered on a strong nucleosome positioning sequence ['601'; (23); W-Nuc165] exhibited the same behaviour in EMSAs as the linker-less A-Nuc147 nucleosomes in the presence of full length and truncated MeCP2 (Figure 2E).

The stoichiometry and histone composition of the nucleosome-MeCP2 complexes was further investigated using SEC-MALS. This method provides information about sample purity and monodispersity (SEC) and a direct measure of the particle molecular weight (MALS). The particle molecular weight is the basis for stoichiometry determination of complexes in solution. MeCP2-WT was added to A-Nuc147 or W-Nuc165 to a point at which over 90% of MeCP2-nucleosome complexes migrating in the first shifted band were obtained at an approximate molar ratio of 1.5 MeCP2 to 1 nucleosome. These samples were injected individually onto a Superose-6 size exclusion column connected to a light scattering detector. Samples containing either full length MeCP2, and A-Nuc147 or W-Nuc165 in the absence of full length MeCP2 were used as controls. Each chromatogram displays a single symmetric peak, indicating the homogeneity of the preparations (Supplementary Figure S2). The analysis of the molar mass at the center part of the peak reveals mono-dispersity for all samples, as evident by the mass distribution line in Supplementary Figure S2 (Table 1). For full length MeCP2, A-Nuc147 and W-Nuc165, the molar mass derived from the center part of the peak measured by light scattering is in close agreement with the respective calculated molecular weight (Table 1). For both nucleosome–MeCP2 complexes, the measured molar mass agreed very well with the calculated molecular weight for a 1:1 molar ratio of nucleosome to MeCP2 (Table 1). These data also show that no histones are released upon interaction with MeCP2.

To better understand the structures of the MeCP2-nucleosome complexes identified by EMSA experiments, we employed sedimentation velocity in the analytical ultracentrifuge (SV-AUC). Full length MeCP2 is a monomer in solution with a sedimentation coefficient of 2.3 S and an anomalously high frictional coefficient due to its intrinsically disordered nature (9). The diffusion-corrected sedimentation coefficient distributions of A-Nuc147 alone and in complex with MeCP2 at two different ratios are shown in Figure 3A. Under our experimental conditions, A-Nuc147 sediments as a homogeneous 11 S species, consistent with earlier studies of isolated nucleosome core particles (35). Quite surprisingly, the 1:1.5 and 1:3.0 MeCP2–A-Nuc147 complexes sedimented more slowly than the nucleosome itself (~10.4 S and ~10.7 S, respectively). Given that a ratio of 1:1.5 produced a 1:1 MeCP2–A-Nuc147 complex (Supplementary Figure S2; see above) and that the sedimentation coefficient of a di-nucleosome is 15 S (36), the SV-AUC data indicate that the 20% increase in molecular weight due to one MeCP2 binding to a single A-Nuc147 is offset by the increase in frictional coefficient of the resulting MeCP2–A-Nuc147 complex. Importantly, the gel shown in Figure 3B was run after the samples had been subjected to SV-AUC. Thus, we conclude that the increase in electrophoretic shifts obtained upon increasing the MeCP2-nucleosome ratio from 1.5 to 3.0 are due to the interaction of one, then additional MeCP2 molecule(s), with a single A-Nuc147.

We repeated the SV-AUC studies with the MeCP2–W-Nuc165 complexes. At a 1:1 molar ratio, the sedimentation coefficient of W-Nuc165 decreased as with A-Nuc147 (Figure 3C). However, at a 2:1 MeCP2 per nucleosome molar ratio, the sedimentation coefficient distribution was extremely heterogeneous and ranged from 12 to >30 S. The electrophoretic behaviour of the two samples is shown in Figure 3D. Thus, binding of MeCP2 to W-Nuc165 leads to both anomalous changes in frictional properties of the complex and protein-dependent 'bridging' of multiple W-Nuc165 particles into higher order aggregates (e.g. dimers, trimers). Taken together, our analyses of the MeCP2–A-Nuc147 and MeCP2–W-Nuc165 complexes indicate that linker DNA is required for bridging, presumably reflecting engagement of multiple MeCP2 DNA binding sites with available extra-nucleosomal DNA segments.

MeCP2 preferentially interacts with nucleosomes containing extra-nucleosomal linker DNA

Previous quantitative studies have observed robust interaction with nucleosomes assembled on longer DNA

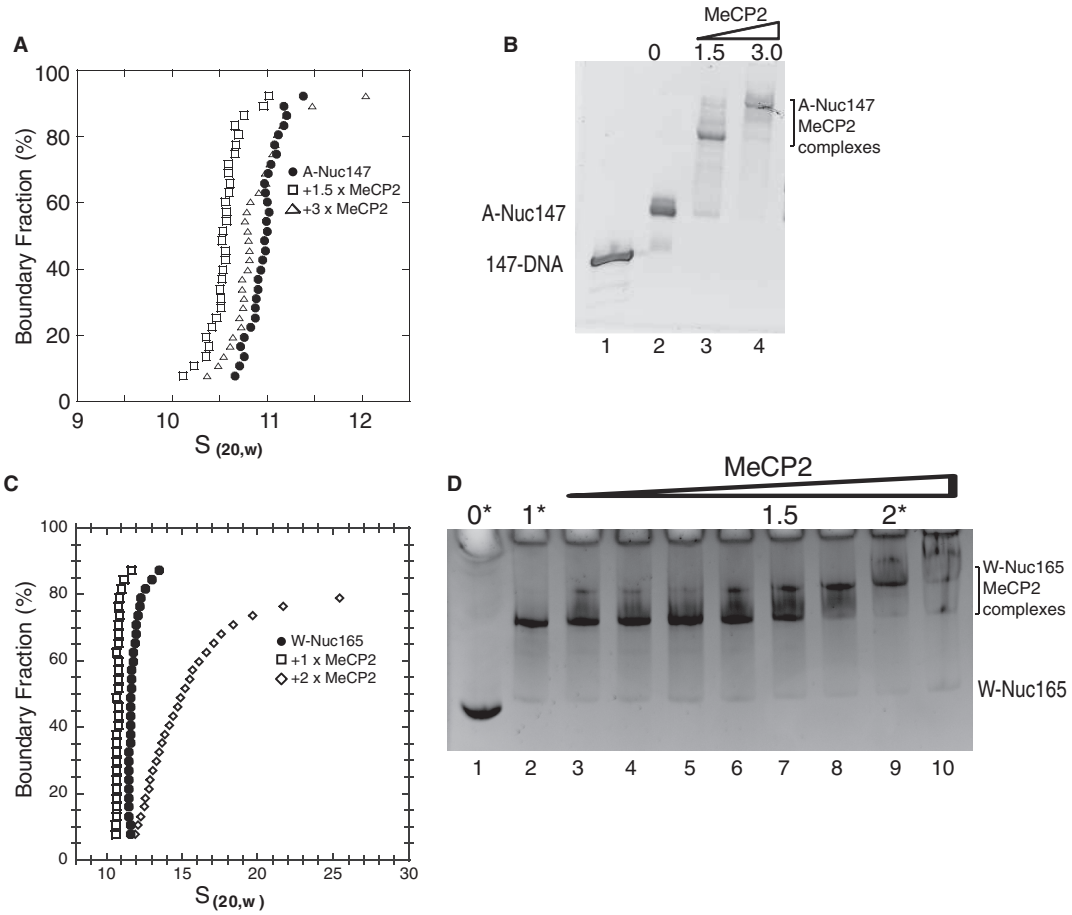

Figure 3. Analytical ultracentrifugation of MeCP2-nucleosome complexes. (**A**) Sedimentation velocity analysis of A-Nuc147 and A-Nuc147-MeCP2 complexes in 20 mM Tris–HCl, pH 7.5, 1 mM EDTA, 1 mM DTT (TCS). Data sets: filled circles A-147Nuc; squares – A-147Nuc-MeCP2 1:1 complex; triangles—A-147Nuc-MeCP2 1:2 complex (**B**) A-Nuc147-MeCP2 complexes analysed in (A) were run on a 5% native gel after the sedimentation experiment and stained with ethidium bromide. The complexes were still intact after the sedimentation experiments. (**C**) Sedimentation velocity analysis of W-Nuc165 and W-Nuc165-MeCP2 complexes, under conditions as described in (A). Filled circles: W-Nuc165, squares: W-Nuc165 with an equimolar amount of MeCP2, diamonds: 2-fold molar excess of MeCP2. (**D**) Ethidium bromide stained 5% native gel of a constant amount of W-Nuc165 titrated with increasing amounts of MeCP2, numbers on the top indicate molar ratios of MeCP2. Asterisks indicate the samples that were analysed by AUC.

fragments containing linker DNA (11,20). To differentiate the relative binding affinities of MeCP2 for nucleosomes with and without linker DNA, we used a competition assay. To exclude possible sequence-dependent differences between the two nucleosomes and to directly investigate the effect of linker DNA on binding affinity, we prepared nucleosomes with the central 146 bp of the 601 sequence used for W-Nuc165 (W-Nuc146; Supplementary Figure S1). W-Nuc146 was pre-incubated with full length MeCP2 at a molar ratio ranging from 1 to 1.5. Increasing amounts of fluorescently labeled W-Nuc165 was added and incubated at room temperature for another 30 min before resolving the complexes by 5% native PAGE. Fluorescently labeled W-Nuc165 successfully competes with W-Nuc146 for MeCP2, as observed in an increase in the amount of W-Nuc165–MeCP2 complex, accompanied by an increase of free W-Nuc146 (Figure 4A, lanes 3–6). This is particularly apparent when only fluorescently labeled W-Nuc165 is visualized (Figure 4B, lanes 4–6). At lower concentrations, all of the W-Nuc165 is found in complex with MeCP2. Conversely, when increasing amounts of W-Nuc146 were added as a competitor to the pre-formed W-Nuc165-MeCP2 complex, the amount of 165NCP-MeCP2 complexes remains nearly unchanged (Figure 4A and B, lanes 8–10).

To investigate whether MeCP2 prefers free DNA over extra-nucleosomal nucleosomal linker DNA, a similar competition assay was performed between W-Nuc165 and a non-nucleosomal 53 bp DNA fragment. Figure 4C demonstrates that addition of free 53 bp DNA to the pre-formed W-Nuc165–MeCP2-WT complex results in a decrease in the amount of W-Nuc165–MeCP2 complex, with a concomitant increase in the amount of W-Nuc165 and newly formed complexes between 53 bp DNA and MeCP2 (Figure 4C, lanes 8–10). Together, our results demonstrate that MeCP2 discriminates against histone-bound nucleosomal DNA and also prefers binding to longer free DNA fragments over the relatively short (10 bp) linker DNA presented in W-Nuc165.

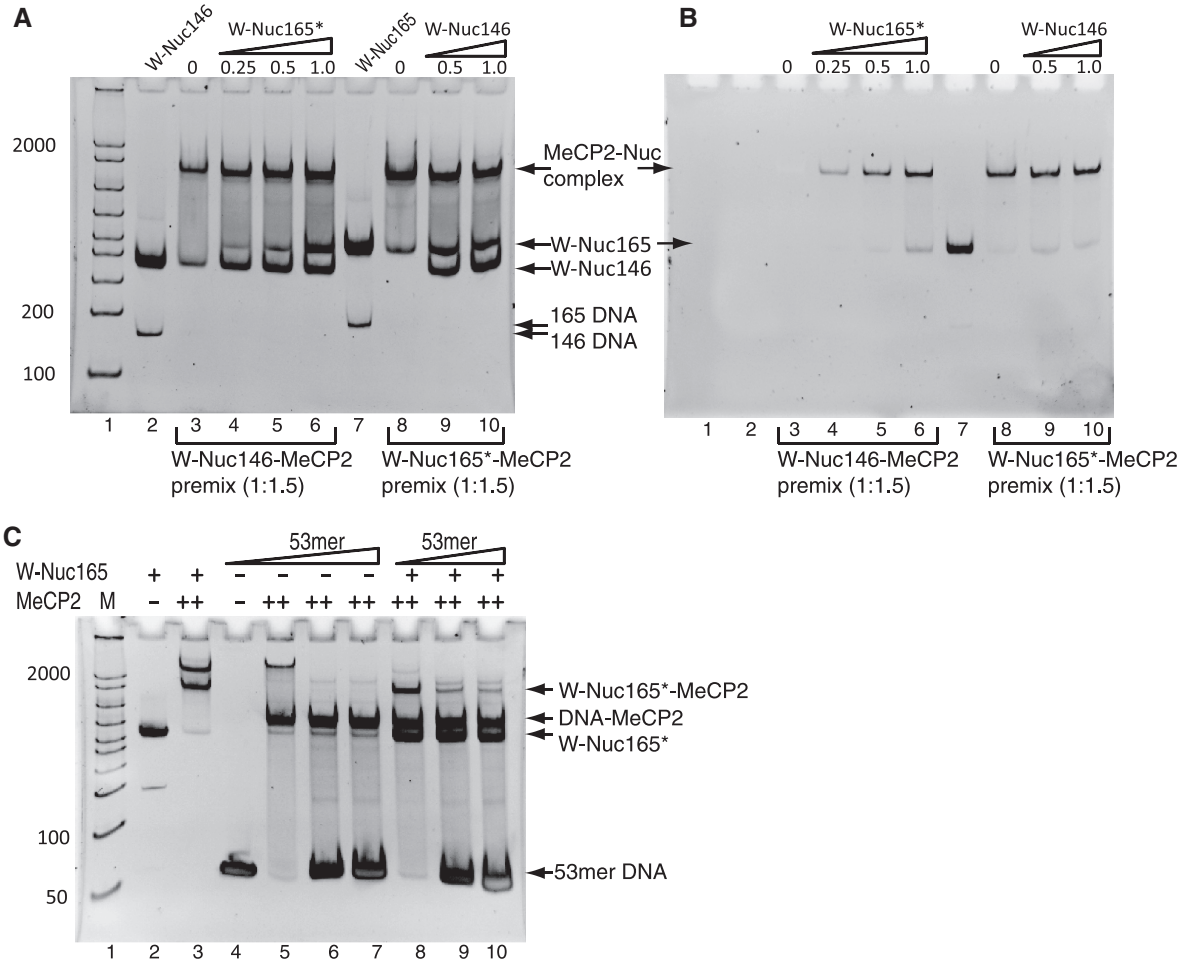

Figure 4. MeCP2 preferentially interacts with nucleosomes with extra-nucleosomal linker DNA. (**A**) MeCP2 was pre-incubated with W-Nuc146, and an increasing amount of fluorescently labeled W-Nuc165 (W-Nuc165*) was added as a competitor (lanes 4–6). In lanes 8–10, W-Nuc146 was added as competitor to pre-incubated W-Nuc165*-MeCP2 complex. (**B**) Fluorescence view of the gel shown in (A), demonstrating the increase in fluorescently labeled 165NCP-MeCP2 complex when W-Nuc165* was added as a competitor (lanes 4–6), but no significant change was observed in lanes 9, 10 when W-146Nuc was added as a competitor. (**C**) Competition assay between 53 bp DNA and W-Nuc165. 53mer DNA was added to pre-incubated W-Nuc165*-MeCP2 complex, resulting in the formation of MeCP2-DNA complexes and free nucleosome (lanes 8–10).

SAXS reveals sequence-dependent differences in DNA conformation in nucleosomes

SAXS provides information on the dimensions and shape of macromolecules in solution. Additionally, structural information can be calculated from SAXS data at 10–50 Å resolution (37,38). We used SAXS to obtain complementary information on nucleosome-MeCP2 complexes. As an important control, we first obtained scattering data from nucleosomes in the absence of MeCP2. While the crystal structure of A-Nuc147 is known to a very high resolution (39) and the structures of W-Nuc146 to medium resolution (40), the structure for W-Nuc165 is not known. The published structures of A-Nuc147 and W-Nuc146 are very similar: both structures show approximately 1.75 turns of double stranded DNA wound around the histone octamer. Figure 5A (based on the A-Nuc147 structure) is representative for both crystal structures. To allow for a direct comparison between nucleosomes with and without linker DNA and to test whether DNA sequence had an effect on overall nucleosome structure in solution, we performed SAXS on all three nucleosomes. The same samples that were used for SAXS were shown to be highly homogeneous using EMSA and by SEC-MALS (Supplementary Figure S2).

Guinier analysis (27) is performed at very low scattering angles and it predicts a linear relationship between ln(I) and s^2, for ideal solutions. From the slope of the line the radius of gyration can be determined. Non-ideal solution behaviour, such as aggregation can be visualized in non-linear components. This analysis demonstrates that none of the nucleosome samples exhibit signs of aggregation; repeat exposure of the same sample shows no sign of radiation damage (data not shown). Inspection of the P(r) data (a histogram of intra-particle vectors) reveals the bell-shaped curves that are characteristic of globular complexes with well-defined maximum particle sizes for all three nucleosome preparations (Supplementary Figure S3). W-Nuc146 (with 601 DNA) displayed a d_{max}

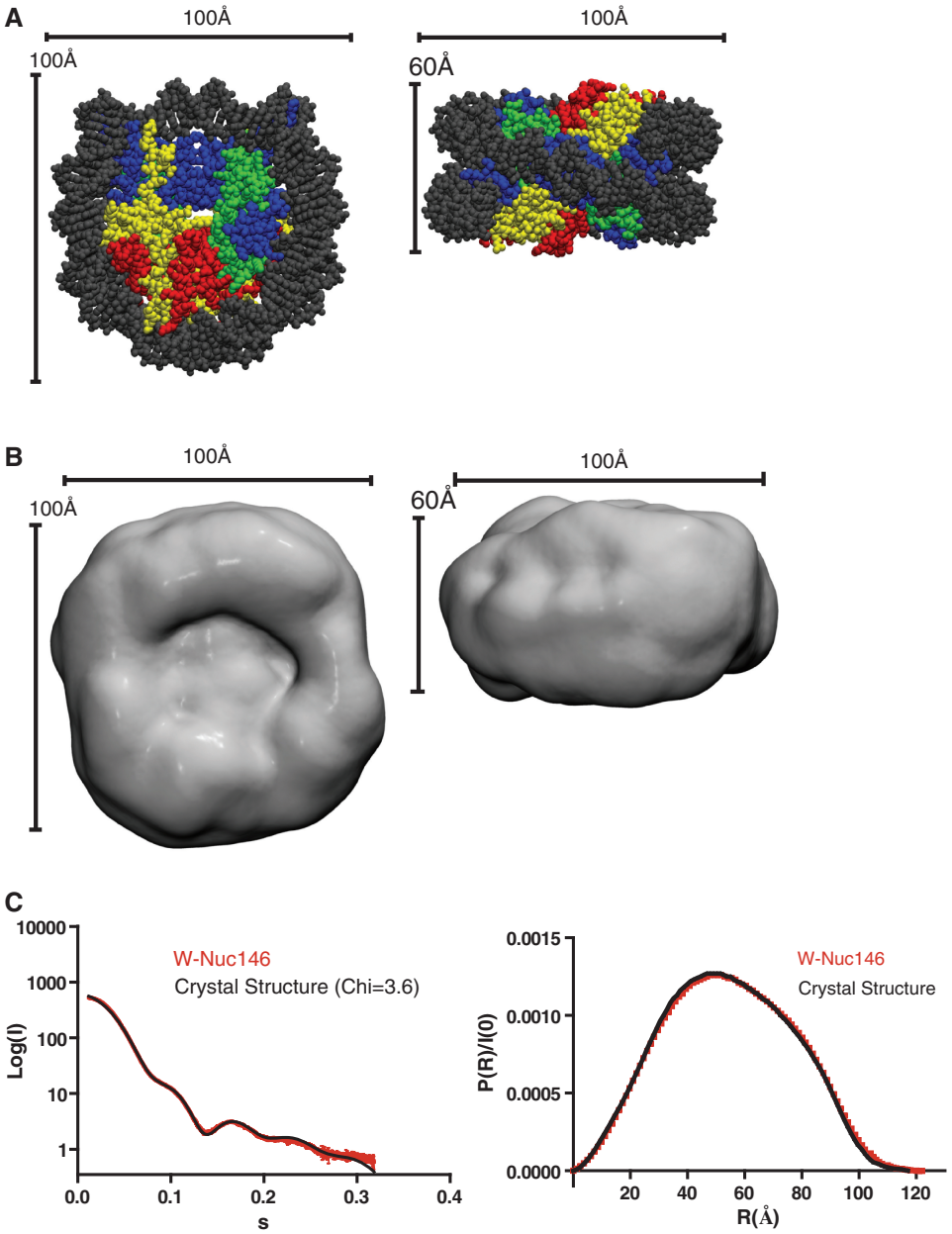

Figure 5. SAXS analysis of W-Nuc146 as a proof of concept**.** (**A**) The crystal structure of the nucleosome core particle [PDB entry 1AOI, (22)], which consists of two copies each of H2A (yellow), H2B (red), H3 (blue), H4 (green) and 147 bp of DNA (gray), with the histone tails removed, serves as a reference. The particle measures approximately $100 \times 100 \times 60$ Å in size. To allow comparison of particle sizes, these size indicators are consistently used in envelope reconstructions in this paper. (**B**) Molecular envelope derived from SAXS data for W-Nuc146. This envelope is an average of ten reconstructions, acquired with the program DAMMIN (29) in slow mode. Movies of these envelopes are available in Supplementary Data, giving a better appreciation of three-dimensional views of these envelopes. (**C**) (Left panel) Experimental scattering data (red) superimposed with simulated data from the crystal structure (black), generated with the program CRYSOL (41) with PDB entry 1AOI as input (histone tails removed from the model). The CRYSOL χ value for the match of the crystal structure with the experimental data is shown in the figure (value in parentheses). (Right panel) The same data after inversion to P(r) functions by the program AUTOGNOM (28). Both graphs show that the crystal structure is an excellent model to explain the experimental scattering data.

of 123 Å, consistent with that obtained from X-ray crystallography (~115 Å; Table 2). The experimental scattering data and the P(r) functions for this particle superimpose very well with scattering data simulated from the nucleosome crystal structure (pdb entry 1AOI, flexible histone tails removed; Figure 5C) using the program CRYSOL (41). The molecular envelope was calculated from the scattering data using the program DAMMIN. The reconstructed image consists of an average of at least 10 individual reconstructions; the individual models agree well with each other, as judged by the normalized spatial discrepancy (see Supplementary Table S1 for statistics associated with averaging). The envelope for W-Nuc146 corresponds closely to the nucleosome crystal structure (compare Figure 5A and B). The nucleosome dyad-region is clearly identifiable in the molecular

Table 2. Rg and d_{max} of MeCP2, nucleosomes and MeCP2-nucleosome complexes, obtained from Small Angle X-ray Scattering

Molecule or complex	Rg (Å)	d_{max} (Å)	Experimental Porod Vol. (10^5) Å^3	Theoretical Vol for $(NCP)_1(MeCP2)_1$ (10^5) Å^3
W-Nuc146 ('601' DNA) [3]	41.6 ± 0.5	123	3.62 ± 0.12	
W-Nuc146-MeCP2 full length	64.7 ± 1.3	222	10.11 ± 0.34	5.2
A-Nuc147 (α-sat DNA) [3]	43.9 ± 0.6	145	3.69 ± 0.13	
A-Nuc147-MeCP2(78-305)	45.5 ± 0.4	156	3.41 ± 0.12	3.9
A-Nuc147-MeCP2 full length	54.7 ± 0.6	194	5.09 ± 0.06	5.2
W-Nuc165 ('601' DNA) [3]	42.1 ± 0.3	148	3.64 ± 0.14	
W-Nuc165–MeCP2(78–305)	43.2 ± 0.2	151	3.98 ± 0.15	3.9
W-Nuc165–MeCP2 full length [2]	46.5 ± 0.1	164	4.36 ± 0.12	5.2
MeCP2(78–305)	37.0 ± 0.9	86	0.22 ± 0.00	
MeCP2 full length	62.5 ± 4.5	198	1.53 ± 0.06	

d_{max} was determined with AUTOGNOM, an automated version of GNOM (28). The number in square brackets lists the number of individual nucleosome preparations and data collection iterations for each sample (if done more than once). Porod volumes and their error estimates were derived from AUTOPOROD (47). The last column in the table lists the expected particle exclusion volumes under the assumption that 1:1 complexes are formed between the nucleosomes and MeCP2.

envelope, since the envelope is narrower at the location of the dyad axis, the only region on the nucleosome where a single layer of DNA double helix is located (Supplementary movie). At the low ionic strength conditions used here, the flexible histone tails do not extend away from the surface of the nucleosome but likely are closely associated with the nucleosomal DNA (42).

A-Nuc147 (with α-sat DNA) is slightly larger (d_{max} of 145 Å; Table 2), indicating differences compared with the corresponding crystal structure. This is also obvious from the comparison of the experimental scattering curve with a scattering curve calculated from the crystal structure (Figure 6B.1). Envelopes calculated from the experimental data show a shape that does not correspond to the crystal structure (compare Figure 6A with Figure 5A). Preparations were carefully checked with native PAGE and SEC-MALS to exclude the possibility of contaminants and inhomogeneity, respectively, and similar results have been obtained from three independent nucleosome preparations. We interpret this changed shape by partial unpeeling of nucleosomal DNA from the histone octamer in at least a significant fraction of the nucleosomes in solution. In forward calculations, a nucleosome with 6–10 bp of DNA unpeeled from the body of the histone octamer gave a much better match to the experimental intensity curve (Figure 6B.1). Furthermore, this interpretation is supported by increased sensitivity of the DNA ends towards micrococcal nuclease digestion compared with W-Nuc146 (Supplementary Figure S4).

The d_{max} of W-Nuc165 was 148 Å, a size that is consistent with expectations from the addition of 7 and 11 bp to the two ends of W-Nuc146 (Table 2). A model in which 7 and 11 bp of DNA were added to either side of the canonical nucleosome is a better match in forward calculations than the crystal structure. An average envelope is shown in Figure 6C.

MeCP2 becomes less extended upon interaction with W-Nuc165

Analysis of the SAXS data for full length MeCP2 further documents that MeCP2 is an extended, largely disordered molecule [Table 2; compare Kratky plots in Supplementary Figure S6 for A-Nuc147, MeCP2 alone and in complex with A-Nuc147; (8)]. The extended nature is also apparent from its P(r) function, which shows many more long intra-particle distances than a globular molecule and a large maximum (linear) particle dimension, d_{max} (Figure 7A). Both features are indicative of an extended molecule. Upon complex formation with A-Nuc147, MeCP2 maintains a rather extended conformation, as seen in the P(r) function of the complex and in a d_{max} of the complex that is 50 Å larger than that obtained for nucleosome alone (Table 2). *Ab initio* calculated envelopes demonstrate that the basic shape of the nucleosome is maintained and display an asymmetric relatively narrow extension which we interpret to be MeCP2 (Figure 7C). Because the structure of full length MeCP2 is unknown and the protein is known to be mostly disordered (9), rigid body modeling of the complex is not feasible. A particle of A-Nuc147 in complex with a fragment of MeCP2 that only contains the first of at least three DNA binding sites [$MeCP2_{(74–305)}$; Figure 1] exhibits only a slightly increased d_{max} compared with the unbound nucleosome (Table 2). This suggests that the DBDs in this entire fragment are engaged in interactions, resulting in a global shape and size for the complex that does not differ significantly from that of the unbound nucleosome. Both of these particles represent 1:1 stoichiometric complexes between MeCP2 and the nucleosome, as verified by SEC-MALS, and consistent with the Porod volumes (Supplementary Figure S2, Table 2).

The volumes calculated for a W-Nuc146-MeCP2 particle suggest that this nucleosome interacts with more than one molecule of full length MeCP2 (its stoichiometry had not been confirmed by SEC-MALS prior to SAXS data collection). The obtained complexes are even more extended than those between full length MeCP2 and A-Nuc147 (Table 2). Finally, the complex between W-Nuc165 and either full length MeCP2 or $MeCP2_{(74–305)}$ is only slightly larger than W-Nuc165 in the absence of MeCP2 (d_{max} of 151 and 164–Å, respectively; Table 2 and Figure 7B). These data suggest that MeCP2 interacts differently with nucleosomes without

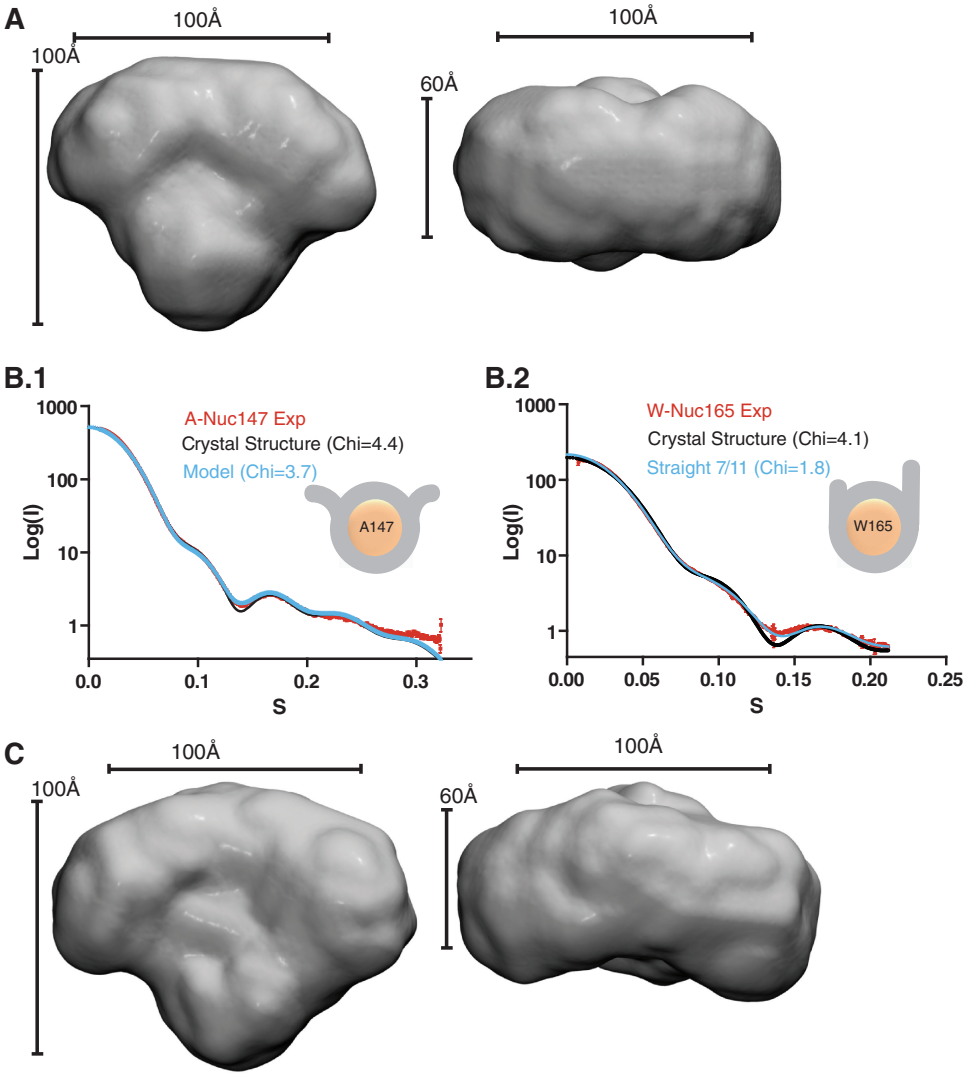

Figure 6. SAXS reveals sequence-dependent conformational heterogeneity in nucleosomes. (**A**) The average molecular envelope reconstructed from SAXS data for A-Nuc147. It is distinctly different from the envelope shown in Figure 5B and has a less round character. (**B.1**) The experimental scattering data for A-Nuc147 (red), simulated data from the crystal structure 1AOI (histone tails removed, black) and simulated data from a model for A-Nuc147 (blue) are superimposed. The CRYSOL χ values for the match of the respective models with the experimental data are shown in parentheses in the figure. A cartoon of a new model for A-Nuc147 is shown in the inset. The model was made by rearranging the terminal six DNA base pairs on each end. (**B.2**) Experimental scattering data for W-Nuc165 (red), simulated data from the crystal structure 1AOI (histone tails removed, black) and simulated data from a model for W-Nuc165 (blue) are superimposed. CRYSOL χ values are shown for each model. A cartoon of the model is shown in the inset. The model was made by extending the DNA by 7 and 11 bp, respectively. (**C**) Average molecular envelope reconstructed for W-165Nuc.

and with linker DNA. Limited proteolysis of nucleosome-bound MeCP2 indeed revealed subtle differences in the protection of MeCP2 bound to W-Nuc146 and W-Nuc165 (Supplementary Figure S5B, C, E and F). MeCP2 bound to W-Nuc146 was degraded more rapidly and with more intermediate bands than MeCP2 bound to W-Nuc165. Together, these data illustrate the unique way in which MeCP2 interacts with the nucleosome, in particular with its linker DNA, and demonstrates the plasticity of MeCP2.

DISCUSSION

MeCP2 is an intrinsically disordered protein for which only limited structural information exists. Here, we present the biophysical and structural characterization of several MeCP2-nucleosome complexes. We demonstrate that one molecule of MeCP2 forms a well-defined complex with nucleosomes with and without extra-nucleosomal linker DNA, without displacing any of the core histones. The molecular dimensions obtained from SAXS experiments demonstrate that MeCP2, which is extended and disordered in its free state, assumes a less extended conformation upon interacting with nucleosomes containing linker DNA, but remains extended when interacting with nucleosomes without DNA linkers. This suggests that additional DNA binding domains in MeCP2 become engaged upon the interaction with linker DNA and nucleosomes. Together, our data allow us to build a working model for MeCP2-nucleosome

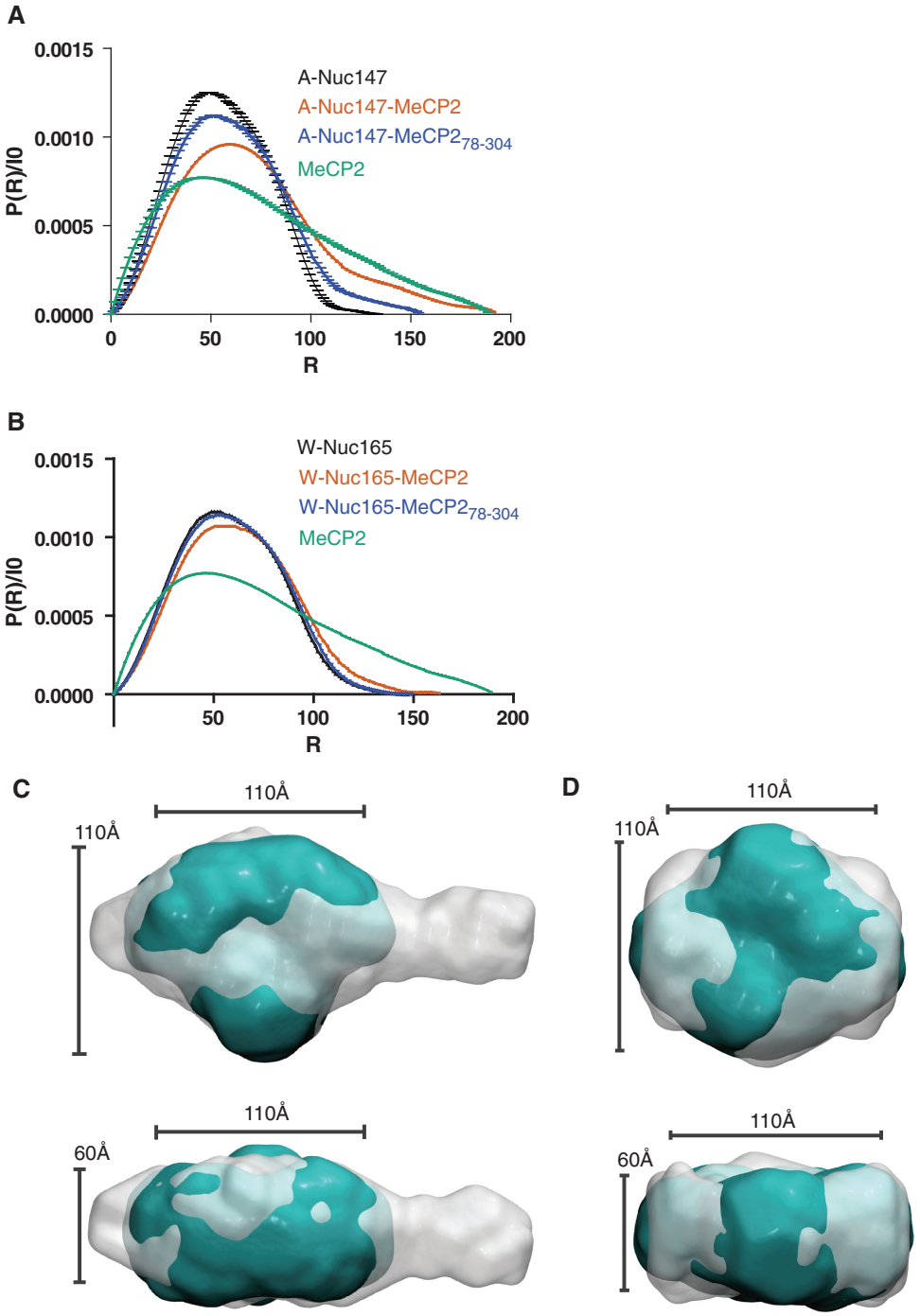

Figure 7. SAXS data show that MeCP2 interacts differently with A-147Nuc compared with W-165Nuc. (**A**) Normalized P(r) functions for A-Nuc147 and complexes with full length and truncated MeCP2 (78–305) show that the complex of the nucleosome and MeCP2 has approximately the same dimension as the sum of its parts. (**B**) Normalized P(r) functions for W-Nuc165 and complexes with full length and truncated MeCP2 show that the complex is similar in size and character to the nucleosome by itself. (**C**) Superposition of average envelopes reconstructed from SAXS data, with the A-Nuc147—MeCP2 complex in transparent gray and the corresponding nucleosome in blue. (**D**) Same as (C) for the W-Nuc165 – MeCP2 complex and W-Nuc165, respectively.

interactions (Figure 8). Finally, SAXS experiments reveal unexpected differences in DNA end conformations between nucleosomes reconstituted with two different DNA sequences.

Ab initio envelope calculations without prior knowledge of the structures can reveal valuable information on the shape of macromolecules at 10–50 Å resolution. It must be pointed out however that protein and DNA have different X-ray scattering properties and as such the approximation of a molecular envelope with uniform density deduced from SAXS of a complex containing both DNA and protein does not strictly hold true. However, our proof

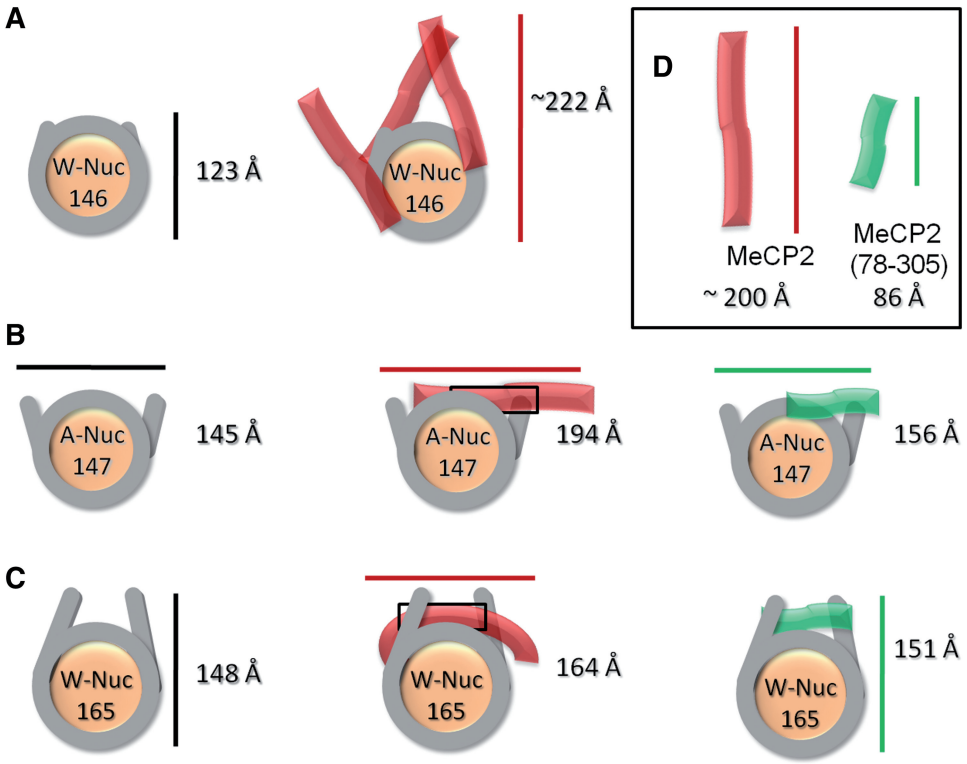

Figure 8. Models for MeCP2–nucleosome interactions: nucleosomes and MeCP2 are shown to scale, according to the d_{max} values determined by SAXS (Table 2). Note that d_{max} for highly extended proteins such as MeCP2 is notoriously difficult to determine. The model takes into account that MeCP2 binds near the nucleosomal dyad. (**A**) W-Nuc146 interacts with multiple copies of full length MeCP2 (as judged from Porod volumes; Table 2) to form extended complexes. (**B**) A-Nuc147 interacts with a single copy of MeCP2 or MeCP2$_{78–305}$ (as shown by SEC-MALS, Supplementary Figure S2), (**C**) W-Nuc165 also forms defined 1:1 complexes with both versions of MeCP2. The relatively minor changes in d_{max} between unbound nucleosomes and those in complex with full length MeCP2 or MeCP2$_{78–305}$ suggests that DNA binding domains in the C-terminal region of MeCP2 are also engaged in interactions with this nucleosome.

of concept SAXS experiment with W-Nuc146 shows a remarkable agreement between the reconstructed envelope and the canonical crystal structure, perhaps with an 'emphasized' density for DNA. The fact that the crystal structure is a good model to predict and explain the scattering data, and that the 3D crystal structure fits the reconstructed envelope well, verifies the reconstruction as a reliable representation of the molecules in solution. Unexpectedly, the A-Nuc147 nucleosome that has been used for crystal structure determination (A-Nuc147) (43) appears to exist in a state in which both terminal 6–10 bp of DNA are dissociated from the histone octamer in solution. This interpretation is supported by increased susceptibility of these nucleosomes to micrococcal nuclease digestion. Our results are consistent with weakened histone–DNA interactions for the terminal base pairs, as predicted from the crystal structure (22) and determined by single molecule experiments (44). The apparent disagreement between the solution state observed for A-Nuc147 and the crystal structure can be explained by the fact that the ends of the DNA are engaged in essential crystal contacts in the crystal lattice (22) and thus the 'closed conformation' is selected during the crystallization process. The observed differences between nucleosomes reconstituted with DNAs with similar lengths, but different sequence suggests a contribution of DNA sequence to nucleosome conformation. It should be pointed out that SAXS data were obtained at very low salt conditions; furthermore, additional DNA sequences must be tested to validate this concept.

Previously SAXS was used to analyse nucleosomes prepared from native tissues, resulting in nucleosomes with a range of DNA sequence and lengths and histone post-translational modifications (42). Nucleosomes with an average DNA length of 146 and 165 bp were shown to have a d_{max} of ~137 Å at low ionic strength, in agreement with the values for A-Nuc147 and W-Nuc165 listed in Table 1. With increasing ionic strength, Mangenot *et al.* (42) found an increase in d_{max}, presumably due to the dissociation of the histone tails from the DNA. The dimensions for the nucleosomes reported here for low-salt conditions are slightly smaller (and in case of W-Nuc146 a better match to the crystal structure) than those published earlier. Later SAXS experiments with recombinant nucleosomes reconstituted with tail-deleted versions of H2A and H2B and full length H3 and H4 on a 146 bp fragment derived from the 5S rRNA gene, resulted in subtly altered scattering curves which were interpreted as a possible partial dissociation of DNA ends (45). These differences occur in the same region of the intensity plot as observed when comparing A-Nuc147 and W-Nuc146 ($0.13 \leq s \leq 0.16$).

It has been reported previously that extra-nucleosomal linker DNA is essential for MeCP2 interactions with

nucleosomes (20). Experiments presented here, performed at higher concentrations of both MeCP2 and nucleosomes, demonstrate the formation of defined complexes with nucleosomes without linker DNA (A-Nuc147). Based on solution studies of these nucleosomes in the absence of MeCP2 (discussed above), we propose that MeCP2 interacts with the partially unpeeled DNA sequences in lieu of linker DNA. In contrast, nucleosomes reconstituted onto 146 bp of 601 sequence have highly ordered and tightly associated DNA ends; these nucleosomes bind several MeCP2 molecules. Because the complex retains an extended conformation, we propose that these interactions are non-specific and not very tight. In direct competition experiments MeCP2 exhibits a clear preference for nucleosomes with linker DNA (e.g. W-Nuc165), and prefers free DNA over these. We conclude that tightly folded nucleosomes (such as W-Nuc146) are a poor substrate for MeCP2, but that DNA partially dissociated from the nucleosome represents a substitute for interaction in the absence of linker DNA. Several histone variants give rise to nucleosomes with less-tightly organized DNA ends [e.g. H2A.Bbd (46); and the centromeric variant of H3, CenpA; K.L. unpublished results], suggesting the hypothesis that MeCP2 might preferentially bind to such variant nucleosomes.

MeCP2 protects ~11 bp of extra-nucleosomal DNA as seen from micrococcal nuclease digestions (20), suggesting that it binds near the nucleosomal dyad axis. Together with our own results that MeCP2 forms a 1:1 complex with a nucleosome that retains all four histones, and based on SAXS data obtained with nucleosome complexes with full length and truncated MeCP2 (Table 2), we can build a tentative working model for the MeCP2–nucleosome complex (Figure 8). As observed previously (8,9) and confirmed here with independent approaches, free MeCP2 exhibits all of the hallmarks of an intrinsically disordered and extended protein. Nucleosomes without linker DNA (W-Nuc146) do not allow specific interactions, resulting in several non-specifically (and presumably weakly bound) MeCP2 molecules (Figure 8A). A-Nuc147 offers only the partially unpeeled nucleosomal DNA for interaction and thus only the MBD and the TRD are engaged in binding, while the remaining 200 amino acids extend into the solvent (Figure 8B). This is sufficient to yield a MeCP2-nucleosome complex with anomalous hydrodynamic properties. Upon interaction with a nucleosome with linker DNA (W-Nuc165), the d_{max} values of the resulting complexes suggest that MeCP2 either becomes more compact or that it engages additional DNA binding sites that are located in the C-terminal half of the protein (Figure 8C). We propose the latter explanation to be more likely, because MeCP2 clearly prefers nucleosomes with linker DNA over linker-less nucleosomes. Together, our data are consistent with a model in which MeCP2 requires at least 2×11 bp of linker DNA for proper engagement of all DNA binding domains. The polyvalent binding of MeCP2 contributes to our understanding of how RTT mutants outside of the MBD (e.g. a truncation at amino acid 294) may result in a diseased state.

SUPPLEMENTARY DATA

Supplementary Data are available at NAR Online.

ACKNOWLEDGEMENTS

Drs Michal Hammel and Robert P. Rambo (ALS) are acknowledged for help in collecting and analysing SAXS and the light scattering data. The authors thank Dr. Steven McBryant for help with SV-AUC experiments, Dr Valerie H. Adams for providing the MeCP2 plasmids; Drs Wayne Lilyestrom, Robert Woody and John Tainer for discussions. The content is solely the responsibility of the authors and does not necessarily represent the official views of the National Institute of General Medical Sciences or the National Institutes of Health.

FUNDING

International Rett Syndrome Foundation and American Heart Association for financial support (to K.L. and C.Y., respectively); Howard Hughes Medical Institute (to K.L.); National Institutes of Health (GM R01GM061909 and GM R01GM096192 to M.J.vdW. and K.L.;) GM R01GM066834 (to J.C.H.); W.M. Keck foundation and Colorado State University (to The W.M. Keck protein expression and purification facility); X-ray scattering and diffraction technologies and their applications to the determination of macromolecular shapes and conformations at the SIBYLS beamline at the Advanced Light Source, Lawrence Berkeley National Laboratory are supported in part by the DOE program Integrated Diffraction Analysis Technologies (IDAT) and the DOE program Molecular Assemblies Genes and Genomics Integrated Efficiently (MAGGIE) under Contract Number DE-AC02-05CH11231 with the U.S. Department of Energy; Efforts to apply SAXS and crystallography to characterize eukaryotic pathways relevant to human cancers are supported in part by National Cancer Institute grant CA92584. Funding for open access charge: Howard Hughes Medical Institute.

Conflict of interest statement. None declared.

REFERENCES

1. Skene,P.J., Illingworth,R.S., Webb,S., Kerr,A.R.W., James,K.D., Turner,D.J., Andrews,R. and Bird,A.P. (2010) Neuronal MeCP2 is expressed at near histone-octamer levels and globally alters the chromatin state. *Mol. Cell*, **37**, 457–468.
2. Chahrour,M. and Zoghbi,H.Y. (2007) The story of Rett syndrome: from clinic to neurobiology. *Neuron*, **56**, 422–437.
3. Hagberg,B. (1985) Retts syndrome - prevalence and impact on progressive severe mental-retardation in girls. *Acta Paediatr. Scand.*, **74**, 405–408.
4. Gonzales,M.L. and LaSalle,J.M. (2010) The role of MeCP2 in brain development and neurodevelopmental disorders. *Curr. Psychiatry Rep.*, **12**, 127–134.
5. Chahrour,M., Jung,S.Y., Shaw,C., Zhou,X.B., Wong,S.T.C., Qin,J. and Zoghbi,H.Y. (2008) MeCP2, a key contributor to neurological disease, activates and represses transcription. *Science*, **320**, 1224–1229.
6. Jones,P.L., Veenstra,G.J.C., Wade,P.A., Vermaak,D., Kass,S.U., Landsberger,N., Strouboulis,J. and Wolffe,A.P. (1998) Methylated

DNA and MeCP2 recruit histone deacetylase to repress transcription. *Nat. Genet.*, **19**, 187–191.
7. Nan,X.S., Ng,H.H., Johnson,C.A., Laherty,C.D., Turner,B.M., Eisenman,R.N. and Bird,A. (1998) Transcriptional repression by the methyl-CpG-binding protein MeCP2 involves a histone deacetylase complex. *Nature*, **393**, 386–389.
8. Klose,R.J. and Bird,A.P. (2004) MeCP2 behaves as an elongated monomer that does not stably associate with the Sin3a chromatin remodeling complex. *J. Biol. Chem.*, **279**, 46490–46496.
9. Adams,V.H., McBryant,S.J., Wade,P.A., Woodcock,C.L. and Hansen,J.C. (2007) Intrinsic disorder and autonomous domain function in the multifunctional nuclear protein, MeCP2. *J. Biol. Chem.*, **282**, 15057–15064.
10. Prilusky,J., Felder,C.E., Zeev-Ben-Mordehai,T., Rydberg,E.H., Man,O., Beckmann,J.S., Silman,I. and Sussman,J.L. (2005) FoldIndex((c)): a simple tool to predict whether a given protein sequence is intrinsically unfolded. *Bioinformatics*, **21**, 3435–3438.
11. Chandler,S.P., Guschin,D., Landsberger,N. and Wolffe,A.P. (1999) The methyl-CpG binding transcriptional repressor MeCP2 stably associates with nucleosomal DNA. *Biochemistry*, **38**, 7008–7018.
12. Kaludov,N.K. and Wolffe,A.P. (2000) MeCP2 driven transcriptional repression in vitro: selectivity for methylated DNA, action at a distance and contacts with the basal transcription machinery. *Nucleic Acids Res.*, **28**, 1921–1928.
13. Wakefield,R.I.D., Smith,B.O., Nan,X.S., Free,A., Soteriou,A., Uhrin,D., Bird,A.P. and Barlow,P.N. (1999) The solution structure of the domain from MeCP2 that binds to methylated DNA. *J. Mol. Biol.*, **291**, 1055–1065.
14. Ho,K.L., Mcnae,L.W., Schmiedeberg,L., Klose,R.J., Bird,A.P. and Walkinshaw,M.D. (2008) MeCP2 binding to DNA depends upon hydration at methyl-CpG. *Mol. Cell*, **29**, 525–531.
15. Fraga,M.F., Ballestar,E., Montoya,G., Taysavang,P., Wade,P.A. and Esteller,M. (2003) The affinity of different MBD proteins for a specific methylated locus depends on their intrinsic binding properties. *Nucleic Acids Res.*, **31**, 1765–1774.
16. Georgel,P.T., Horowitz-Scherer,R.A., Adkins,N., Woodcock,C.L., Wade,P.A. and Hansen,J.C. (2003) Chromatin compaction by human MeCP2 - Assembly of novel secondary chromatin structures in the absence of DNA methylation. *J. Biol. Chem.*, **278**, 32181–32188.
17. Ghosh,R.P., Nikitina,T., Horowitz-Scherer,R.A., Gierasch,L.M., Uversky,V.N., Hite,K., Hansen,J.C. and Woodcock,C.L. (2010) Unique Physical Properties and Interactions of the Domains of Methylated DNA Binding Protein 2. *Biochemistry*, **49**, 4395–4410.
18. Kumar,A., Kamboj,S., Malone,B.M., Kudo,S., Twiss,J.L., Czymmek,K.J., LaSalle,J.M. and Schanen,N.C. (2008) Analysis of protein domains and Rett syndrome mutations indicate that multiple regions influence chromatin-binding dynamics of the chromatin-associated protein MECP2 in vivo. *J. Cell Sci.*, **121**, 1128–1137.
19. Nikitina,T., Shi,X., Ghosh,R.P., Horowitz-Scherer,R.A., Hansen,J.C. and Woodcock,C.L. (2007) Multiple modes of interaction between the methylated DNA binding protein MeCP2 and chromatin. *Mol. Cell. Biol.*, **27**, 864–877.
20. Nikitina,T., Ghosh,R.P., Horowitz-Scherer,R.A., Hansen,J.C., Grigoryev,S.A. and Woodcock,C.L. (2007) MeCP2-chromatin interactions include the formation of chromatosome-like structures and are altered in mutations causing Rett syndrome. *J. Biol. Chem.*, **282**, 28237–28245.
21. Ishibashi,T., Thambirajah,A.A. and Ausio,J. (2008) MeCP2 preferentially binds to methylated linker DNA in the absence of the terminal tail of histone H3 and independently of histone acetylation. *Febs Lett.*, **582**, 1157–1162.
22. Luger,K., Mader,A.W., Richmond,R.K., Sargent,D.F. and Richmond,T.J. (1997) Crystal structure of the nucleosome core particle at 2.8 angstrom resolution. *Nature*, **389**, 251–260.
23. Lowary,P.T. and Widom,J. (1998) New DNA sequence rules for high affinity binding to histone octamer and sequence-directed nucleosome positioning. *J. Mol. Biol.*, **276**, 19–42.
24. Dyer,P.N., Edayathumangalam,R.S., White,C.L., Bao,Y.H., Chakravarthy,S., Muthurajan,U.M. and Luger,K. (2004) Reconstitution of nucleosome core particles from recombinant histones and DNA. *Method Enzymol.*, **375**, 23–44.
25. Demeler,B. and van Holde,K.E. (2004) Sedimentation velocity analysis of highly heterogeneous systems. *Anal. Biochem.*, **335**, 279–288.
26. Konarev,P.V., Volkov,V.V., Sokolova,A.V., Koch,M.H.J. and Svergun,D.I. (2003) PRIMUS: a Windows PC-based system for small-angle scattering data analysis. *J. Appl. Crystallogr.*, **36**, 1277–1282.
27. Guinier,A. and Fournet,F. (1955) *Small angle scattering of X-rays*. Wiley Interscience, New York.
28. Svergun,D.I. (1992) Determination of the regularization parameter in indirect-transform methods using perceptual criteria. *J. Appl. Crystallogr.*, **25**, 495–503.
29. Svergun,D.I. (1999) Restoring low resolution structure of biological macromolecules from solution scattering using simulated annealing. *Biophys. J.*, **76**, 2879–2886.
30. Kozin,M.B. and Svergun,D.I. (2001) Automated matching of high- and low-resolution structural models. *J. Appl. Crystallogr.*, **34**, 33–41.
31. Volkov,V.V. and Svergun,D.I. (2003) Uniqueness of ab initio shape determination in small-angle scattering. *J. Appl. Crystallogr.*, **36**, 860–864.
32. Wriggers,W., Milligan,R.A. and McCammon,J.A. (1999) Situs: A package for docking crystal structures into low-resolution maps from electron microscopy. *J. Struct. Biol.*, **125**, 185–195.
33. Wriggers,W. and Chacon,P. (2001) Using situs for the registration of protein structures with low-resolution bead models from X-ray solution scattering. *J. Appl. Crystallogr.*, **34**, 773–776.
34. Humphrey,W., Dalke,A. and Schulten,K. (1996) VMD: visual molecular dynamics. *J. Mol. Graphics*, **14**, 33–38.
35. van Holde,K.E. (1988) *Chromatin*. Springer-Verlag, New York.
36. Butler,P.J.G. and Thomas,J.O. (1998) Dinucleosomes show compaction by ionic strength, consistent with bending of linker DNA. *J. Mol. Biol.*, **281**, 401–407.
37. Putnam,C.D., Hammel,M., Hura,G.L. and Tainer,J.A. (2007) X-ray solution scattering (SAXS) combined with crystallography and computation: defining accurate macromolecular structures, conformations and assemblies in solution Q. *Rev. Biophys.*, **40**, 191–285.
38. Hura,G.L., Menon,A.L., Hammel,M., Rambo,R.P., Poole II,F.L., Tsutakawa,S.E., Jenney,F.E. Jr, Classen,S., Frankel,K.A., Hopkins,R.C. *et al.* (2009) Robust, high-throughput solution structural analyses by small angle X-ray scattering (SAXS). *Nat. Meth.*, **6**, 606–612.
39. Davey,C.A. and Richmond,T.J. (2002) DNA-dependent divalent cation binding in the nucleosome core particle. *Proc. Natl Acad. Sci. USA*, **99**, 11169–11174.
40. Vasudevan,D., Chua,E.Y.D. and Davey,C.A. (2010) Crystal Structures of Nucleosome Core Particles Containing the '601' Strong Positioning Sequence. *J. Mol. Biol.*, **403**, 1–10.
41. Svergun,D., Barberato,C. and Koch,M.H.J. (1995) CRYSOL - a program to evaluate x-ray solution scattering of biological macromolecules from atomic coordinates. *J. Appl. Crystallogr.*, **28**, 768–773.
42. Mangenot,S., Leforestier,A., Vachette,P., Durand,D. and Livolant,F. (2002) Salt-induced conformation and interaction changes of nucleosome core particles. *Biophys. J.*, **82**, 345–356.
43. Richmond,T.J. and Davey,C.A. (2003) The structure of DNA in the nucleosome core. *Nature*, **423**, 145–150.
44. Hall,M.A., Shundrovsky,A., Bai,L., Fulbright,R.M., Lis,J.T. and Wang,M.D. (2009) High-resolution dynamic mapping of histone-DNA interactions in a nucleosome. *Nat. Struct. Mol. Biol.*, **16**, 124–129.
45. Bertin,A., Durand,D., Renouard,M., Livolant,F. and Mangenot,S. (2007) H2A and H2B tails are essential to properly reconstitute nucleosome core particles. *Eur. Biophys. J.*, **36**, 1083–1094.
46. Bao,Y.H., Konesky,K., Park,Y.J., Rosu,S., Dyer,P.N., Rangasamy,D., Tremethick,D.J., Laybourn,P.J. and Luger,K. (2004) Nucleosomes containing the histone variant H2A.Bbd organize only 118 base pairs of DNA. *EMBO J.*, **23**, 3314–3324.
47. Petoukhov,M.V., Konarev,P.V., Kikhney,A.G. and Svergun,D.I. (2007) ATSAS 2.1 – towards automated and websupported small-angle scattering data analysis. *J. Appl. Crystallogr.*, **40**, s223–s228.